Journal of Magnetic Resonance **147,** 226–231 (2000)
doi:10.1006/jmre.2000.2202, available online at http://www.idealibrary.com on IDEAL®

A Novel Approach to Separating EPR Lines Arising from Species with Different Transition Moments

Wulf Hofbauer and Robert Bittl

Max-Volmer-Institut für Biophysikalische Chemie und Biochemie, Technische Universität Berlin, 10623 Berlin, Germany

E-mail: Robert.Bittl@TU-Berlin.DE

Received April 4, 2000; revised July 31, 2000

In pulsed EPR, spectral contributions from several species in one sample can be separated based on different EPR transition probabilities. This is usually done by monitoring the Rabi nutations in a 2D experiment. By using long pulses, the FID and echo shapes of species with different transition probabilities differ significantly, including temporal shifts of the observed echo signals in a two-pulse ESE experiment. These shifts can be used to disentangle spectral components in a 1D field-swept ESE experiment by choosing an appropriate detection time. This approach is demonstrated by experiments on a sample containing Mn^{2+} and Cr^{3+} centers as well as on an exchange-coupled Mn(III)/Mn(IV) system with Mn^{2+} contaminations. © 2000 Academic Press

Key Words: **EPR; spin dynamics; transition moments; spin multiplicities.**

1. INTRODUCTION

In EPR experiments, samples often contain several inequivalent paramagnetic species. This is sometimes due to an inherent heterogeneity of the sample. Often, undesired EPR signals are also caused by contamination of the sample with paramagnetic impurities. This is common in high-field/high-frequency EPR where Mn^{2+} background signals are virtually unavoidable.

Pulsed EPR can be used to separate signals of species with different relaxation times T_1 or T_2 (see, e.g., (*1*)). In addition, it can be used to distinguish species that differ in their EPR transition moments by analyzing Rabi nutation frequencies (*2, 3*) along the lines of NMR experiments (*4*). In most experiments, the timing of a pulse sequence is varied to record the Rabi nutation via a free induction decay (FID) (see, e.g., (*5, 6*)) or an echo (see, e.g., (*7*)). While these 2D experiments allow a detailed analysis of the occuring Rabi frequencies, the necessary timing variation makes them expensive in terms of acquisition time.

Here we present a novel approach to separating EPR spectra of species with different EPR transition moments in a fast 1D two-pulse echo experiment. While more limited in scope than the established 2D experiments, it is well suited to separate spectral contributions due to contamination of a sample with other paramagnetic species. In addition, it is applicable in cases where short relaxation times restrict the timing variation required for 2D experiments.

2. THEORY

EPR experiments are commonly described in a $[xyz]$ reference frame rotating with the frequency of the applied microwave in the laboratory system (*8*).

The Zeeman interaction of the spin S in the laboratory system $[XYZ]$ ($z = Z$) with the externally applied static magnetic field B_0 is described by the Hamiltonian

$$\hat{H}_0 = -\gamma B_0 \hat{S}_Z, \qquad [1]$$

where γ is the gyromagnetic ratio. In the rotating $[xyz]$ frame, this Hamiltonian is transformed to

$$\hat{H}_0' = -\gamma\left(B_0 - \frac{\omega_{\mathrm{MW}}}{\gamma}\right)\hat{S}_z = -\gamma B_0' \hat{S}_z. \qquad [2]$$

If the microwave frequency is resonant with the EPR transition, B_0' vanishes. Otherwise, it causes the magnetization vector of the spin ensemble to precess about the z axis with the residual Larmor frequency $\omega_0 = \gamma \cdot B_0'$.

The interaction with the applied microwave is described by

$$\hat{H}_1 = -\gamma B_1 \hat{S}_X \cdot \cos\,\omega_{\mathrm{MW}} t \qquad [3]$$

in the laboratory system and is transformed to

$$\hat{H}_1' = -\gamma\,\frac{B_1}{2}\,\hat{S}_x + \hat{H}_1'' \approx -\gamma B_1' \hat{S}_x \qquad [4]$$

in the $[xyz]$ system where $\hat{H}_1''$ contains rapidly oscillating terms and can in general be neglected.

For vanishing B_0', i.e., in the resonant case, the magnetization undergoes transient nutations about the x axis. In the

1090-7807/00 $35.00

following, we consider only a two-level subspace for one EPR transition with the basis $\{|m\rangle, |m+1\rangle\}$. This is a good approximation if this subspace is decoupled from the neglected eigenstates, i.e., other transitions are off-resonant due to additional interactions, e.g., zero field splitting. In the case of an isolated effective Kramers doublet within a spin state of multiplicity $2S+1$, the Rabi frequency for the precession about x is

$$\omega_1 = \gamma B_1' \sqrt{S(S+1) - m(m+1)}. \qquad [5]$$

If this subspace is treated as a $S = \frac{1}{2}$ two-level system, the apparent coupling strengths to the static field B_0 and the oscillating transversal field B_1 differ.

A common two-pulse echo experiment starts at thermal equilibrium where the magnetization is parallel to the z axis. A first short microwave pulse flips the magnetization about the x axis by 90° and generates a FID. The decay of the transversal magnetization is due in part to relaxation. Another cause is dephasing of the magnetic dipole moments in the ensemble due to a distribution of ω_0 for individual spins (inhomogeneous broadening). After a delay τ, another short microwave pulse flips the magnetization by 180° about the x axis. For the xy magnetization this corresponds to a change of the sign of B_0'. Therefore, the dephasing process of the magnetization due to inhomogeneous broadening is reversed, leading to an echo of the initial FID.

The flip angle for a pulse is determined by the Rabi frequency ω_1 and the duration of the pulse. Since ω_1 is given by Eq. [5], the flip angle of a given pulse can be different for species with different S.

To illustrate this, we consider the $m_S = -\frac{1}{2} \leftrightarrow +\frac{1}{2}$ transitions of a $S = \frac{1}{2}$ and a $S = \frac{5}{2}$ system. If the other transitions of the $S = \frac{5}{2}$ system are off-resonant, the Rabi frequencies for these species differ according to Eq. [5] by a factor of 3. Therefore a 90°–τ–180° pulse sequence for the $S = \frac{1}{2}$ system corresponds to a 270°–τ–540° sequence for the $S = \frac{5}{2}$ system. A 270° pulse generates an FID with opposite sign compared to a 90° pulse. Therefore, the respective echoes differ in their signs.

For short, "hard" microwave pulses, the echoes of both species can be regarded as two mirror images of the FID back to back and occur simultaneously. Separation into individual contributions is impossible. However, for long, "soft" pulses this is no longer true. For a review of effects of extended time excitation, see, e.g., (*1*, *9*). In general, the echo shape becomes asymmetric and rather complex for long pulses.

Now we consider an extended time $\Phi = 270°$ pulse (Fig. 1, top) for the $S = \frac{5}{2}$ system. The free induction signal following the long pulse deviates from a monotonous decay and has a maximum occuring at a time t' after the end of the long pulse.

An explanation for this effect can be given by considering the single 270° pulse as a combination of a $\Phi_1 = 90°$ and a $\Phi_2 = 180°$ pulse without a delay in between. An "equivalent" pulse sequence can be constructed by substituting the Φ_1–($\tau = 0$)–Φ_2 pulse sequence by a Φ_1'–τ'–Φ_2' echo sequence with hard Φ_1' and Φ_2' pulses positioned at the centers of the Φ_1 and Φ_2 pulses, respectively (Fig. 1, bottom). This sequence with the same effective flip angle $\Phi_1' + \Phi_2' = 270°$ results in an echo delayed by a time t' which corresponds to half the duration of the $\Phi_1 = 90°$ pulse after the end of the $\Phi_2 = 180°$ pulse. This echo contributes to the observed FID after the single long $\Phi = 270°$ pulse.

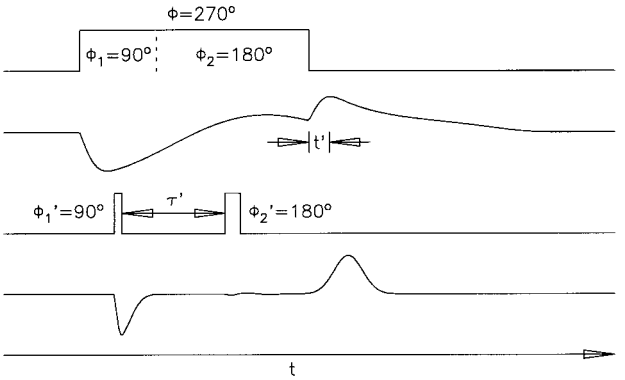

FIG. 1. A time-extended 270° pulse and resulting magnetization (top). The 270° pulse can be split into a 90° and a 180° pulse. An equivalent pulse sequence with short pulses gives rise to an echo (bottom). The maximum FID signal occurs at a delay t' after the end of the long pulse. This is analogous to the echo signal for the sequence with short pulses.

The echo and therefore the delay of the FID maximum occurs only if the total flip angle is large enough to be partitioned into a two-pulse echo sequence. For the same "soft" pulse with a total flip angle of 90°, as in the case of an $S = \frac{1}{2}$ system, no delay of the FID maximum is observed.

Adding another microwave pulse after a delay τ generates an echo of the FID following the first pulse. The delay t' of the FID after a 270° pulse causes a corresponding shift t'' of the echo to earlier times compared to the echo of the FID after a 90° pulse. Another way to describe this effect is to again decompose the first pulse into a 90°–180° sequence and interpret the final echo as the first refocused echo of a Carr–Purcell sequence (*10*).

The illustrative decomposition of a 270° pulse into a 90°–180° pseudo sequence is not the only possible partitioning scheme. For a correct analysis of spin dynamics, a C++ program has been written. It calculates the evolution of the magnetization for arbitrary pulse sequences, neglecting relaxation. Apart from a numerical integration to account for inhomogeneous broadening, the Liouville–von Neumann equation is thereby solved analytically.

Figure 2 shows the calculated magnetization for a two-pulse echo experiment at different nominal flip angles. Due to inhomogeneous broadening, there is a distribution of flip angles within the spin ensemble. Therefore, even for small nominal flip angles, the observed echo amplitude generally starts out

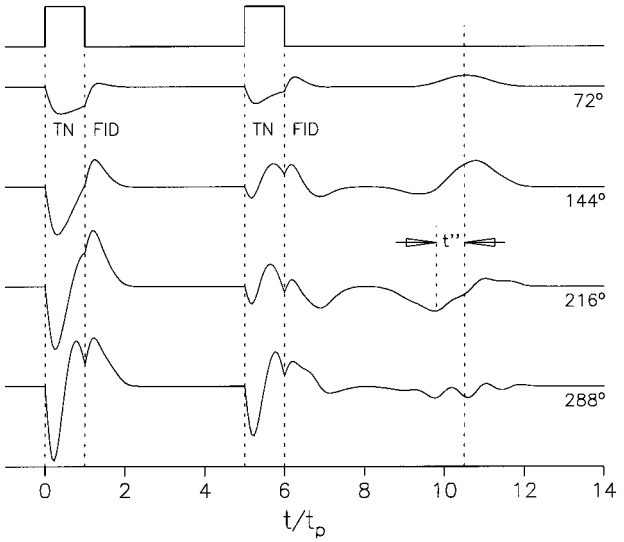

FIG. 2. Solid-state echo sequence (top) and resulting y magnetization for flip angles of 72, 144, 216, and 288° (top to bottom). The shape and position of the echo signal changes significantly as a function of the flip angle. The time axis is relative to the pulse length t_p.

negative, changes sign, and ends positive, reflecting subensembles with flip angles larger or smaller than 180°. The ratio of the negative and positive parts as well as the time of the zero crossing change as a function of the nominal flip angle. For very large nominal flip angles, the echo becomes oscillatory due to a multimodal flip angle distribution. The shift of the echo discussed before is most noticeable in the simulation for a nominal flip angle of 216°.

The time dependence of the minima, zero crossings, and maxima of the echoes as a function of the nominal flip angle is shown in Fig. 3. Flip angles of 72, 144, and 216° have been marked. These are the same angles used in the simulations in Fig. 2. The 3:2:1 ratio of the flip angles corresponds to the transition moments of the $m_S = -\frac{1}{2} \leftrightarrow +\frac{1}{2}$ transitions in systems with a total spin of $S = \frac{1}{2}$, $S = \frac{3}{2}$, or $S = \frac{5}{2}$. The time of the zero crossing varies by about twice the pulse length used. It is therefore possible to choose a detection time where the signal of one spin state is suppressed while others are maintained. Figure 3 illustrates this situation for two positions of the detection window. At $t/t_p \approx 9.8$, indicated by a dashed vertical line, the zero crossing of the echo arises for an $S = \frac{3}{2}$ state. At the same time, the echo signals for $S = \frac{5}{2}$ and $S = \frac{1}{2}$ remain. At $t/t_p \approx 10.7$ the echo signal for an $S = \frac{3}{2}$ state is at its maximum while the echo for an $S = \frac{5}{2}$ state has a zero crossing. Therefore, the overlapping spectra associated with these flip angles can be fully disentangled in a field-swept electron spin echo (ESE) experiment by the choice of the detection time window. Figure 4 shows the echo shapes for these flip angles in detail together with suitable integration windows (shaded areas).

Since all time-dependent information can be recorded in one shot and detection windows be applied numerically *after* data

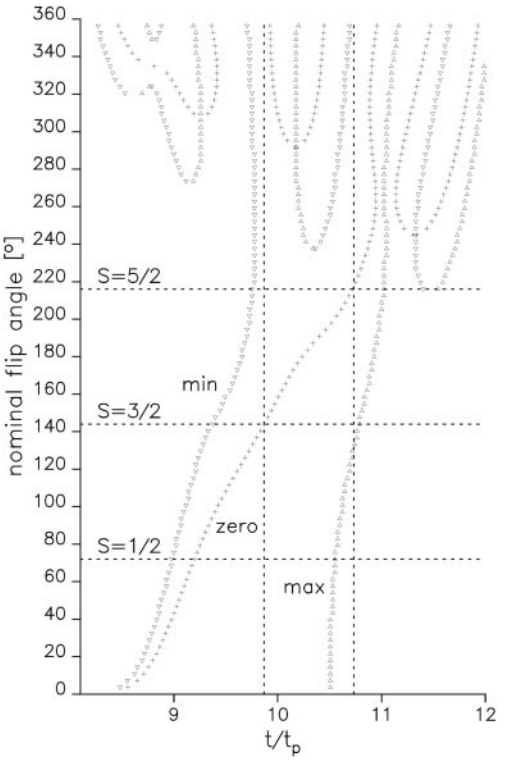

FIG. 3. Dependence of echo signal minima (∇), maxima (Δ), and zero crossings (+) on the nominal flip angle for the echo sequence in Fig. 2. The time axis is relative to the length t_p of the microwave pulses. Flip angles with a 3:2:1 ratio corresponding to $S = \frac{5}{2}$, $S = \frac{3}{2}$, and $S = \frac{1}{2}$, respectively, are marked by dashed horizontal lines. The times indicated by dashed vertical lines correspond to the $S = \frac{5}{2}$ ($\Phi = 216°$) and the $S = \frac{3}{2}$ ($\Phi = 144°$) zero crossings, respectively.

acquisition, this method is a 1D experiment in terms of acquisition time. The only difference to a standard field-swept ESE experiment is the recording of the entire echo trace and the addition of an off-line signal processing step.

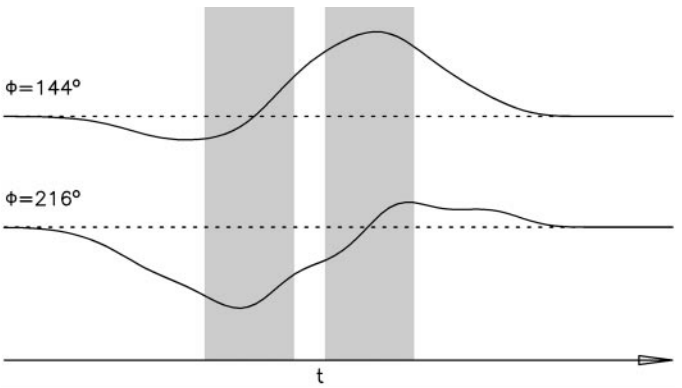

FIG. 4. Two echo shapes for nominal flip angles of $\Phi = 144°$ and $\Phi = 216°$. Integration time windows based on the data in Fig. 3 to detect one signal while suppressing the other are indicated as shaded regions.

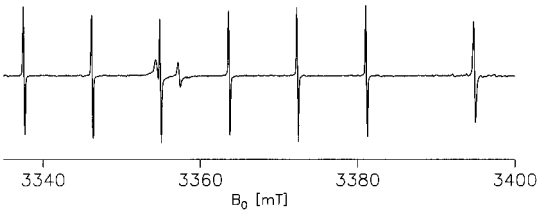

FIG. 5. cw EPR spectrum of a CaO sample with Mn^{2+} and Cr^{3+} centers ($T = 40$ K). The six major lines below $B_0 = 3385$ mT arise from Mn^{2+}; the line at $B_0 = 3394$ mT with small satellites is a Cr^{3+} contribution.

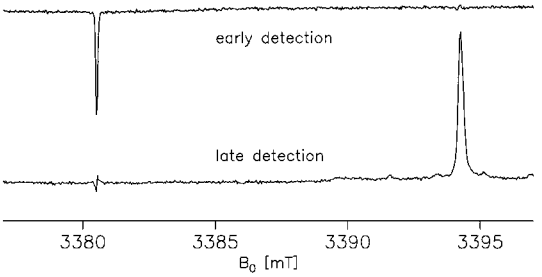

FIG. 6. Field-swept ESE spectra of the sample with the cw spectrum shown in Fig. 5 in the range 3377–3397 mT. The top trace has been obtained by using an early echo integration window and shows the inverted highest field line of Mn^{2+} while the Cr^{3+} line is suppressed. The bottom trace shows the Cr^{3+} line (including $^{53}Cr^{3+}$ satellites) with a virtually eliminated Mn^{2+} line by using a late echo integration window.

3. EXAMPLES

The suggested technique has been experimentally tested and successfully applied to several systems. Here, we show two examples: (i) separation of Mn^{2+} ($S = \frac{5}{2}$) and Cr^{3+} ($S = \frac{3}{2}$) centers in powdered CaO, and (ii) elimination of Mn^{2+} ($S = \frac{5}{2}$) contamination signals in an exchange-coupled $S = \frac{1}{2}$ Mn(III)–Mn(IV) complex.

3.1. Experimental Setup

All experiments were performed using an Elexsys 680 (Bruker) pulsed 94-GHz spectrometer. The mixer design of the spectrometer limits the available microwave power to less than 5 mW. Typical pulse lengths are therefore rather long (about 200 ns) and well suited to achieve the desired effect.

For both samples, a field-swept ESE experiment was performed. A solid-state echo sequence (two identical pulses) was used. The specific choice of pulse lengths was rather uncritical as long as the nominal flip angle was smaller than 180° for one species and larger than 180° for the other. The resulting echo signal was recorded with a transient recorder. The experiment was controlled by Xepr software (Bruker) and a custom PulseSpeL (Bruker) script.

To simulate a boxcar integration of the echo signal, the raw data set was convolved with a rectangular window function along the time axis. From the resulting 2D data set, those time slices with optimal separation of the individual signal contributions were selected. This approach is particularly useful because it is rather difficult to adjust the nominal flip angles to precisely known values with soft pulses. These processing steps were performed with standard functions built into Xepr.

3.2. Samples

3.2.1. Mn^{2+} and Cr^{3+} in CaO. For this experiment, a Mn^{2+}:CaO calibration sample delivered with the spectrometer was used. The diamagnetic CaO powder contains Mn^{2+} centers ($S = \frac{5}{2}$, $I = \frac{5}{2}$) giving rise to a six-line EPR spectrum commonly used for calibrating the magnetic field. The sample also contains Cr^{3+} centers ($S = \frac{3}{2}$, $I = 0$), resulting in a single EPR line with weak satellites due to the natural abundance of ^{53}Cr ($I = \frac{3}{2}$). A cw spectrum of the sample is shown in Fig. 5.

Only the $m_S = -\frac{1}{2} \leftrightarrow m_S = +\frac{1}{2}$ transitions contribute to the observed narrow lines for both species. Therefore, the $m_S = \pm\frac{1}{2}$ sublevels are sufficiently decoupled to treat them as two-level systems. The Rabi frequency ratio for both species is then $\omega_{1,Mn}/\omega_{1,Cr} = \frac{3}{2}$.

The Mn^{2+} and Cr^{3+} contributions have no spectral overlap. The clear spectral separation of the species is most instructive to demonstrate the principle of the experiment.

The field-swept ESE spectrum was acquired with a pulse length of 350 ns at maximum pulse power and an interpulse delay of 2.5 μs. The range of the magnetic field was restricted to include only the Mn^{2+} line occuring at the highest field and the Cr^{3+} line. The shapes of the echoes differ noticeably for Mn^{2+} and Cr^{3+} (Fig. 7) and closely resemble the simulated echo shapes in Fig. 4.

A time window of 480 ns was used for numerical integration after the measurement. Figure 6 shows the resulting spectrum for two optimum choices of the window position (see Fig. 4). The Cr^{3+} signal is completely suppressed for the early integration window while maintaining the Mn^{2+} signal (Fig. 6, top trace). For the later detection window, the Mn^{2+} signal is suppressed while the Cr^{3+} line (including the $^{53}Cr^{3+}$ satellites) becomes visible (Fig. 6, bottom trace). Therefore, the desired separation could be achieved, despite the rather small ratio of the respective Rabi frequencies.

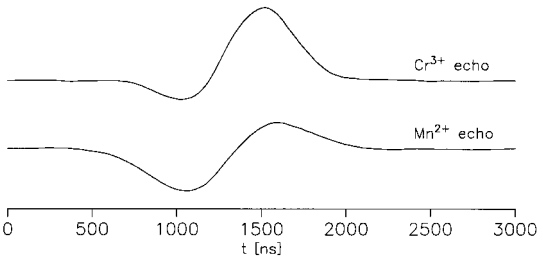

FIG. 7. Echo shapes in a two-pulse echo experiment with long pulses on the sample with the cw spectrum shown in Fig. 5. In the top trace, the Cr^{3+} transition is on resonance ($B_0 = 3394.2$ mT) while in the bottom trace the highest field line of Mn^{2+} is resonant ($B_0 = 3380.5$ mT).

3.2.2. DTNE. The usefulness of the described method for a typical sample with spectral overlap of different species is illustrated by EPR experiments on an Mn(III)Mn(IV) exchange-coupled system ([(dtne)Mn(III)μ-OAc(μ-O)$_2$Mn(IV)]$^{2+}$). The electron spins of both manganese atoms are anti-ferromagnetically coupled to a total spin $S = \frac{1}{2}$ (*11*). Contamination with Mn^{2+} is almost inevitable as manganese is a constituent of the complex.

The EPR signal of the complex is spread out over a large spectral range (more than 100 mT) while the Mn^{2+} contamination yields the well-known six intense lines over a range of about 50 mT. The Rabi frequency ratio of both components is $\omega_{1,Mn}/\omega_{1,DTNE} = 3$.

Attempts to separate the species based on different relaxation rates failed at $T = 20$ K because T_1 and T_2 were too short to allow for a significant change of the pulse timing. For the same reason in combination with the rather low microwave power available, observing Rabi nutations in a 2D experiment as in (*5*) was not possible. In order to obtain a sufficient signal intensity, it was necessary to minimize the length of the pulse/detection sequence as far as possible, i.e., down to a value where the FID of the second pulse and the echo signal were just separated.

Figure 8 shows spectra taken with two different integration windows. The window positions correspond approximately to the times indicated in Fig. 3. For the later detection time, the $S = \frac{5}{2}$ signal is completely suppressed (top trace). At the earlier time, a superposition of both $S = \frac{1}{2}$ and $S = \frac{5}{2}$ signals is visible (bottom trace). To suppress the $S = \frac{1}{2}$ component and obtain a spectrum of the Mn^{2+} contamination only, it would be necessary to use an even earlier detection window.

Figure 9 compares a cw spectrum of the same sample to the derivative of the pulse echo spectrum with suppressed Mn^{2+} lines. Since the Mn^{2+} lines are very narrow compared to the EPR lines of the complex and their transition moments are large, the cw EPR spectrum of the complex is impaired even by extremely small concentrations of Mn^{2+}. The derivative of the echo spectrum exhibits only very minor rests of the Mn^{2+} signal. Those parts of the spectra that are unaffected by Mn^{2+} impurities are identical to each other. This agreement corroborates that the ESE experiment, despite the unusual integration window, yields an undistorted spectrum of the DTNE complex.

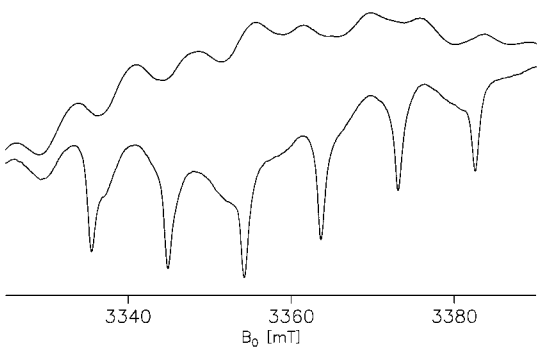

FIG. 8. ESE spectra of the DTNE complex at $T = 20$ K for two different integration windows. The integration window for the top trace was optimized for suppression of the Mn^{2+} contributions.

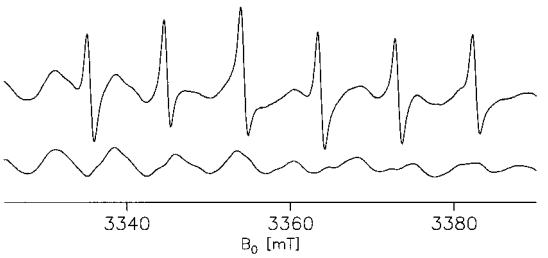

FIG. 9. Top: cw spectrum of the DTNE complex at $T = 20$ K. Only the part of the spectrum affected by Mn^{2+} impurities is shown. Bottom: Derivative of the ESE spectrum with an integration window optimized to eliminate the Mn^{2+} lines.

4. CONCLUSION

The use of long microwave pulses in spin-echo experiments can lead to significant distortion and temporal shifts of the observed echo. It has been shown both theoretically and experimentally that this effect can be used to separate signals deriving from species with different transition moments.

This method is very easy to implement as it is a standard two-pulse echo experiment with acquisition of the whole echo trace. The timing of the pulse sequence remains fixed during the experiment. As all time-dependent information is gathered in one shot, the benefit of separating signals of species with different Rabi nutation frequencies is free in terms of acquisition time.

The required data analysis, i.e., the numerical integration of the echo signal after acquisition, can easily be implemented in software. The choice of the integration windows for best separation of the species can be based on simulations like those in Fig. 3 and further refined interactively when distinctive spectral features of one of the species are known (as in the case of contamination signals), without needing to repeat the experiment. It should also be possible to describe the observed echo shape as a superposition of theoretical echo shapes for different flip angles and therefore disentangle more than two spectra.

Beside the two examples shown here, the suggested method has been successfully applied in our laboratory to several other systems and proven its particular usefulness to eliminate Mn^{2+} contamination signals in high-frequency EPR.

ACKNOWLEDGMENTS

The authors thank Prof. Wieghart (Max-Planck-Institut für Strahlenchemie, Mülheim) and Kai Schäfer (TU Berlin) for the DTNE sample and W. Lubitz for his support. Financial support by Deutsche Forschungsgemeinschaft (Bi 464/7-1) and Fonds der Chemischen Industrie (to RB) is gratefully acknowledged.

REFERENCES

1. A. Schweiger, *Angew. Chem.* **103,** 223–250 (1991).
2. M. K. Bowman, in "Modern Pulsed and Continuous-Wave Electron Spin Resonance" (L. Kevan and M. K. Bowman, Eds.), Wiley, New York, 1990.
3. A. V. Astashkin and A. Schweiger, *Chem. Phys. Lett.* **174,** 595–602 (1990).
4. H. C. Torrey, *Phys. Rev.* **76,** 1059–1068 (1949).
5. J. Isoya, H. Kanda, J. R. Norris, J. Tang, and M. K. Bowman, *Phys. Rev. B* **41,** 3905–3913 (1990).
6. T. Takui, K. Sato, D. Shiomi, K. Itoh, T. Kaneko, E. Tsuchida, and H. Nishide, *Mol. Cryst. Liq. Cryst.* **279,** 155–176 (1996).
7. S. Stoll, G. Jeschke, M. Willer, and A. Schweiger, *J. Magn. Reson.* **130,** 86–96 (1998).
8. J. A. Weil, J. R. Bolton, and J. E. Wertz, "Electron Paramagnetic Resonance: Elementary Theory and Practical Applications," Wiley, New York, 1994.
9. A. Schweiger, in "Modern Pulsed and Continuous-Wave Electron Spin Resonance" (L. Kevan and M. K. Bowman, Eds.), Wiley, New York, 1990.
10. H. Y. Carr and E. M. Purcell, *Phys. Rev.* **94,** 630–638 (1954).
11. K.-O. Schäfer, R. Bittl, W. Zweygart, F. Lendzian, G. Haselhorst, T. Weyhermüller, K. Wieghardt, and W. Lubitz, *J. Am. Chem. Soc.* **120,** 13104–13120 (1998).